Partially Magnetized Plasma Instabilities in a Three-Dimensional Particle-in-Cell Simulation

IEPC-2024-852

Presented at the 38th International Electric Propulsion Conference, Toulouse, France
June 23-28, 2024

Andrew Denig[*] and Kentaro Hara[†]
Stanford University, Stanford, CA, 94305, United States of America

Several kinetic instabilities exist in partially magnetized plasmas, including electron cyclotron drift instability (ECDI) and modified two-stream instability (MTSI). The fluctuation-based electron transport that results from these MHz frequency waves is seemingly responsible for the anomalous transport of electrons across magnetic fields lines in cross-field devices like Hall effect thrusters. A three-dimensional (3D) particle-in-cell study was conducted for a periodic box with perpendicular, applied electric and magnetic fields to investigate ECDI and MTSI in a 3D configuration. A short-wavelength mode propagating in the $\mathbf{E} \times \mathbf{B}$ direction immediately develops that matches the linear perturbation theory of ECDI very closely. As this instability saturates, the waves within the domain transfer their energy to a long-wavelength mode that propagates at a 45° angle in the x-y plane. More analysis is required to determine the physical mechanism of this wave's creation, but the quantitative agreement of the ECDI theory and the initial short-wavelength mode provides reason to believe that this long-wavelength mode is also physical.

Nomenclature

$\mathbf{B}$ = magnetic field
$\mathbf{E}$ = electric field
γ = growth rate
$I_n(x)$ = modified Bessel function of the first kind of order n
$k_\parallel$ = wavevector component parallel to the magnetic field
$k_\perp$ = wavevector component perpendicular to the magnetic field
k = magnitude of wavevector $\mathbf{k}$
λ_D = Debye length
ω = complex frequency
ω_{ce} = electron cyclotron frequency
ω_{pi} = ion plasma frequency
ω_r = real frequency
r_L = Larmor radius
$\mathbf{U}_d$ = $\mathbf{E} \times \mathbf{B}$ drift velocity
$v_{th,e}$ = electron thermal speed
$Z(\xi)$ = plasma dispersion function

---

[*] PhD Candidate, Aeronautics and Astronautics, adenig3@stanford.edu.
[†] Assistant Professor, Aeronautics and Astronautics, kenhara@stanford.edu.

I. Introduction

Hall effect thrusters[1] (HETs) are cross-field devices that employ perpendicular electric and magnetic fields to trap electrons, that ionize an injected stream of neutral atoms, typically xenon, to produce thrust. The efficiency of such systems is dependent on the confinement of these electrons within the discharge chamber. However, numerical simulations[2–5] and experimental evidence[6] have demonstrated that high-frequency, short wavelength modes are present within the discharge chamber and plume of the HET. It has been hypothesized that these oscillations lead to turbulence-based, anomalous electron transport across magnetic field lines that is an order of magnitude greater than what would be expected from collisions alone. Because the modes of interest are short-wavelength (< 1 mm), several kinetic instabilities are of interest, including electron cyclotron drift instability (ECDI)[7,8] and modified two-stream instability (MTSI).[9,10] ECDI and MTSI are electrostatic, kinetic instabilities that are driven by the relative drift of the unmagnetized ions with respect to the magnetized electrons. ECDI propagates in the $\mathbf{E}\times\mathbf{B}$ direction, while MTSI also has a long-wavelength component parallel to the magnetic field.

Understanding the contribution of this plasma turbulence to the axial transport of electrons requires detailed numerical modeling that are able to capture the behavior of both ions and electrons as they interact with the waves initiated by the plasma instabilities. These plasma instabilities are inherently three-dimensional (3D), as they depend on phenomena parallel to the magnetic field, like MTSI and Landau damping, as well as phenomena perpendicular to the magnetic field, like the electron gyromotion and the $\mathbf{E}\times\mathbf{B}$ drift of electrons with respect to ions. Many two-dimensional (2D) simulations have been done[11,12] that capture the radial-azimuthal plane or the axial-azimuthal plane. The radial-azimuthal simulations can capture plasma dynamics along the magnetic field, but the direct impact of the instabilities on the anomalous, axial transport of electrons cannot be studied. On the other hand, the axial-azimuthal simulations can directly capture the enhanced electron transport along the electric field by the waves, but the plasma dynamics parallel to the magnetic field are not included in the study. Furthermore, these 2D simulations are only able to capture lower-dimensional limits of the 3D kinetic theory underlying ECDI and MTSI.[13,14] The weakness of each type of 2D simulation motivates the development of 3D kinetic models. Taccogna[15] and Villafana[16] have previously published 3D particle-in-cell (PIC) models in a geometry representative of a Hall effect thruster and found that amplitude and behavior of the plasma waves differ between 2D and 3D simulations. These studies motivate a simplified, 3D test case that can be used to study the development of electrostatic, kinetic instabilities and can provide a direct, numerical verification of the three-dimensional, linear instability theory of ECDI and MTSI.

II. Linear Perturbation Theory: Partially Magnetized Plasmas

For the following theory and simulation, the electric field is in the x direction (axial), $\mathbf{E} = E_0\hat{x}$, the magnetic field is in the z direction (radial), $\mathbf{B} = B_0\hat{z}$, and the $\mathbf{E}\times\mathbf{B}$ direction is in the $-y$ direction (azimuthal). The two electrostatic, kinetic instabilities of interest in partially magnetized plasmas are ECDI and MTSI. Because of the $\mathbf{E}\times\mathbf{B}$ drift experienced by the electrons relative to the ions, the electron population acquires a bulk velocity of magnitude E/B. ECDI occurs when the Doppler-shifted, electron Bernstein modes couple to the ion acoustic mode.[10] The maximum growth rate occurs for $k_z = 0$ such that the wave propagates purely in the plane normal to the magnetic field. MTSI arises from the same phenomenon as ECDI, but it is also characterized by some finite wave propagation along the magnetic field lines, i.e., $k_z \neq 0$ with $k_\perp \lambda_D$ small, typically less than 0.2. As a result, both waves can be encapsulated by a single, electrostatic dispersion relation for partially magnetized plasmas, given by Eq. (1):

$$0 = 1 - \frac{\omega_{pi}^2}{\omega^2} + \frac{1}{k^2\lambda_D^2}\left[1 + \frac{\omega - \mathbf{k}\cdot\mathbf{U}_d}{\sqrt{2}k_\parallel v_{th,e}} \times\ e^{-k_\perp^2 r_L^2} \sum_{n=-\infty}^{\infty} I_n(k_\perp^2 r_L^2) Z\left(\frac{\omega - \mathbf{k}\cdot\mathbf{U}_d + n\omega_{ce}}{\sqrt{2}k_\parallel v_{th,e}}\right)\right]. \tag{1}$$

Equation (1) cold, singly-charged ions and warm, magnetized electrons. Furthermore, it is assumed that the bulk velocity of ions is zero, but if there is a nonzero bulk velocity, this would simply Doppler shift ω in the ion susceptibility and not affect the overall physics. In this analysis, the wavenumber $\mathbf{k}$ is real, and the angular frequency $\omega = \omega_r + i\gamma$ is complex.

To isolate the MTSI mode from the ECDI dispersion relation, it can be assumed that $|\omega - \mathbf{k}\cdot\mathbf{U}_d| \ll \omega_{ce}$ such that only the $n = 0$ mode remains in the electron susceptibility:

$$0 = 1 - \frac{\omega_{pi}^2}{\omega^2} + \frac{1}{k^2\lambda_D^2}\left[1 - e^{-k_\perp^2 r_L^2} - \frac{1}{2}e^{-k_\perp^2 r_L^2} I_0(k_\perp^2 r_L^2) Z'\left(\frac{\omega - \mathbf{k}\cdot\mathbf{U}_d}{\sqrt{2}k_\parallel v_{\mathrm{th,e}}}\right)\right]. \tag{2}$$

Eq. (2) yields non-trivial solutions for $k_\parallel \neq 0$. The growth rate as a function of wavenumber resembles the dispersion relation of the traditional two-stream instability, hence the name modified two-stream instability (MTSI), despite the physical origin of the instabilities being quite different.

Techniques for determining the numerical solution of Eq. (1) and Eq. (2) for $\omega(k)$ have been discussed in Refs. 13 and 14. In a Hall effect thruster, the magnetic field in the plasma bulk largely points in the radial direction, perpendicular to the inner and outer walls of the discharge channel. As the unmagnetized ions diffuse toward the walls, along the magnetic field lines, this is hypothesized to set up a nonzero k_z mode within the discharge channel.[11] Therefore, even though the ECDI mode of fastest growth exists for $k_z = 0$, the plasma dynamics fix k_z based on the device scale in the radial direction, permitting both ECDI and MTSI to exist for finite k_z.

III. Numerical Model

A. Code Description

To study the characteristics of ECDI and MTSI in cross-field devices, a 3D, explicit, electrostatic PIC model has been developed in C++. This code is parallelized using MPI to perform domain decomposition. Poisson's equation is numerically solved by the linear solvers package called HYPRE.[17]

1. *Poisson Solver*

Poisson's equation can be discretized in 3D as follows:

$$\frac{\phi_{i-1,j,k} - 2\phi_{i,j,k} + \phi_{i+1,j,k}}{\Delta x^2} + \frac{\phi_{i,j-1,k} - 2\phi_{i,j,k} + \phi_{i,j+1,k}}{\Delta y^2} + \frac{\phi_{i,j,k-1} - 2\phi_{i,j,k} + \phi_{i,j,k+1}}{\Delta z^2} = -\frac{\rho_{i,j,k}}{\epsilon_0}. \tag{3}$$

The generalized minimal residual (GMRES) algorithm is used to solve Poisson's equation for all boundary conditions. The matrix system is preconditioned using the pipe flow multi-grid (PFMG) preconditioner. Each time step, the Poisson solver is run up to 40 iterations, or once the residual of the solution, $||b - A\phi_n||$, has reached 10^{-12}. The Poisson solver was verified using the method of exact solutions for a prescribed right-hand side for both Dirichlet and periodic boundary conditions. For the periodic boundary conditions, a value of ρ/ϵ_0 equal to $12\pi^2\cos(2\pi x)\cos(2\pi y)\cos(2\pi z)$ such that $\phi(x, y, z) = \cos(2\pi x)\cos(2\pi y)\cos(2\pi z)$ was tested, for a domain given by $(x, y, z) \in [0, 1]^3$ m. The resulting potential profile is given in Fig. 1(a).

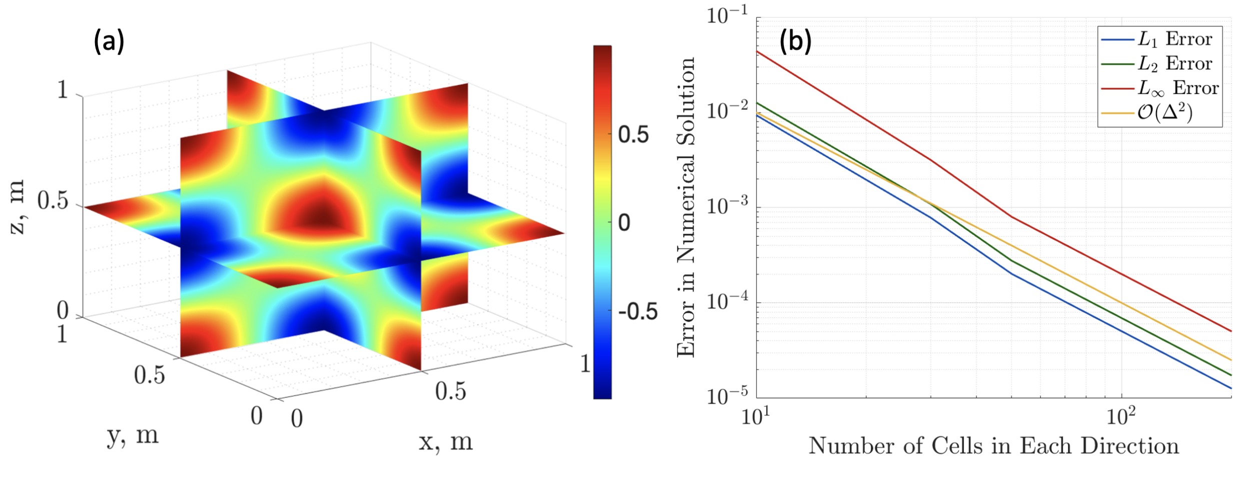

Figure 1. (a) The electric potential in a 3D, periodic box for $\rho/\epsilon_0 = 12\pi^2\cos(2\pi x)\cos(2\pi y)\cos(2\pi z)$. (b) The relative error in ϕ as a function of number of cells in each direction.

For a case with 256 cells in every direction, the absolute error was on the order of 10^{-5} V. Furthermore, while keeping the domain the same size and increasing the number of cells, it was demonstrated that the L_1, L_2, and L_∞ norms all scaled like second-order in the grid spacing. This trend is illustrated in Fig. 1(b).

2. Particle Push, Gather, and Scatter

In addition to solving Poisson's equation for the electric potential and subsequently calculating the electric field, the three main are gathering the electric field to the macroparticles' locations, updating the positions and momenta of all the macroparticles, and scattering the macroparticle information to the cell centers to calculate the fluid quantities, i.e., density, fluid velocity, temperature, etc. Each component of the electric field lies on its own staggered grid with respect to the electric potential. The x-component lies on the y-z faces of each cell, the y-component lies on the x-z faces, and the z-component lies on the x-y faces. Macroparticles near the boundary require electric field information from the neighboring processors. To gather each component of the electric field to the locations of each macroparticle, MPI communication with 18 unique cores is necessary.

Once the electric field at the location of each macroparticle is determined, the momenta for each macroparticle can be updated using the Boris push scheme. With the updated values of momenta, the positions for each particle can be updated using the leapfrog scheme: $x_p^n = x_p^{n-1} + v_p^{n+1/2}\Delta t$. Macroparticles are tallied as they cross processor boundaries, and their weight, position, and velocity are communicated in non-blocking MPI send/receive messages.

All fluid quantities are interpolated from the macroparticles' locations to the cell centers by bi-linear interpolation with examples given for density and x-momentum flux in Eqs. (4) and (5):

$$n_{i,j,k} = \frac{W_p}{\Delta x \Delta y \Delta z} \sum_p S\left(\frac{x_p - X_i}{\Delta x}\right) S\left(\frac{y_p - Y_j}{\Delta y}\right) S\left(\frac{z_p - Z_k}{\Delta z}\right). \tag{4}$$

$$(nu_x)_{i,j,k} = \frac{W_p}{\Delta x \Delta y \Delta z} \sum_p v_{x,p} S\left(\frac{x_p - X_i}{\Delta x}\right) S\left(\frac{y_p - Y_j}{\Delta y}\right) S\left(\frac{z_p - Z_k}{\Delta z}\right). \tag{5}$$

Here, (x_p, y_p, z_p) are the coordinates of the p-th macroparticle, (X_i, Y_j, Z_k) are the coordinates of the (i,j,k)-th cell center, W_p is the macroparticle weight, or the number of real particles per macroparticle, Δx, Δy, and Δz are the cell sizes in each direction, and S is the linear shape function between 0 and 1 that is nonzero for all cell centers bounding the dual cell that contains the p-th macroparticle. The macroparticle weight is assumed to be constant for each particle. In 3D, the macroparticle weight is divided amongst 8 neighboring cell centers. To scatter all macroparticle information in a given processor to the appropriate cell centers in other processors, MPI communication with 26 unique cores is necessary.

B. Code Verification: Two-Stream Instability

The main verification study that combines all subroutines within the 3D PIC code is the electrostatic two-stream instability. For two, equal density beams of electrons moving through each other with a fixed ion background, the dispersion relation is given by Eq. (6):

$$1 - \frac{\omega_{pb}^2}{(\omega - kV_b)^2} - \frac{\omega_{pb}^2}{(\omega + kV_b)^2} = 0. \tag{6}$$

Here, ω_{pb} is the plasma frequency for the beam, and V_b is the beam velocity. The theoretical maximum growth rate is $\gamma = \omega_{pb}/\sqrt{8}$ at a wavenumber of $k_{max} = \sqrt{3/8}\omega_{pb}/V_b$. The density of each beam is 2.5×10^{16} m^{-3} such that the beam plasma frequency is 9×10^9 rad/s. A time step of 10^{-12} s is used to obey the inequality $\omega_{pb}\Delta t < 0.2$. The simulation is run for 4 ns. V_b is chosen to be the thermal velocity of 15 eV electrons, or 1.62×10^6 m/s. The domain length is 2 mm, and there are 128 cells in every direction with 50 macroparticles initialized in every cell.

The electrostatic energy, $|E|^2$ is plotted as a function of time in Fig. 2. The initial positions of the electrons are uniformly randomly sampled. Eventually, the numerical noise in the simulation is sufficient to cause charge bunching, creating an electric field that reinforces this bunching, and so on. This process causes a net transfer of energy from the particles to the field. The linear growth stage of the instability is evident from 0.75 ns to 1.5 ns, before Landau damping saturates the instability. After 1.5 ns, the phase space of

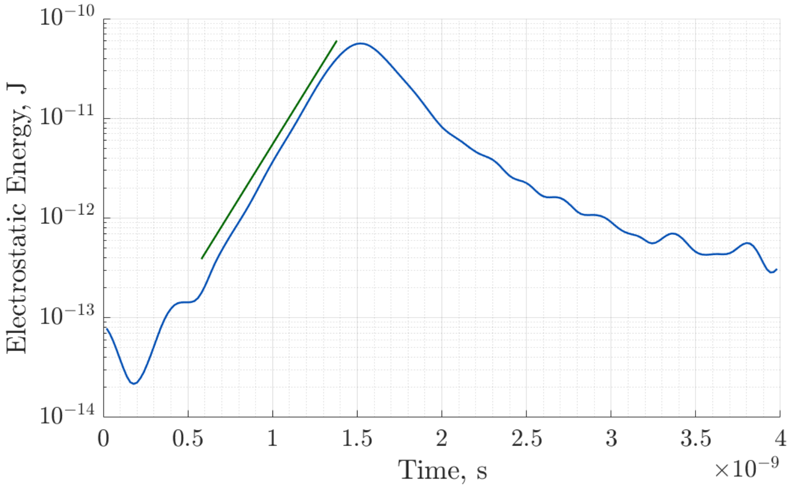

Figure 2. The blue line shows the electrostatic energy of the system as a function of time. The analytical growth rate of $\gamma = \omega_{pb}/\sqrt{8}$ is shown in green.

the electrons is described by the phase mixing characteristic of Landau damping. A grid resolution study was also performed which demonstrated that the linear instability growth rate more closely matched theory as the number of grid points increased. The correct computation of the numerical two-stream growth rate verified the 3D PIC model that was developed.

IV. Results

A. Cross-Field Model Description

Having verified the 3D PIC code, the main test case of interest is a three-dimensional, periodic box with perpendicular, applied electric and magnetic fields. The numerical parameters are given in Table 1.

Table 1. Table of simulation and plasma parameters for the 3D cross-field instability test case.

Plasma Parameter	Value
Applied Electric Field	$7520\ \hat{x}$ V/m
Applied Magnetic Field	$0.015\ \hat{z}$ T
Density	$5 \times 10^{16}\ m^{-3}$
Initial T_e	25 eV
Initial T_i	0.25 eV
Ion Species	Helium

Simulation Parameters	Value
Domain Length ($L_x = L_y = L_z$)	0.02 m
Number of Cells ($N_x = N_y = N_z$)	128
Time Step	5 ps
Simulation Time	4 μs
Particles per Cell per Species	100

The time step was chosen to thoroughly satisfy the heuristic $\max(\omega_{pe}, \omega_{ce})\Delta t < 0.2$. For this case, $\max(\omega_{pe}, \omega_{ce})\Delta t$ is 0.06. Helium ions are considered instead of xenon ions to decrease the simulation time required for the instabilities to saturate. Furthermore, to prevent the unmagnetized ions from gaining unlimited energy from the continuous acceleration along the electric field, the ions are only accelerated under the force of the perturbed electric field, i.e., $E' = E - E_0$, where E_0 is the applied electric field given in Table 1. The ions and electrons are both initialized with a Maxwellian velocity distribution function with temperatures given by Table 1. The positions of both species are initially uniformly sampled within the domain.

B. Simulation Results

Assuming cold ions, the dispersion relation for ECDI and MTSI, given by Eq. (1) is numerically solved for the plasma parameters given in Table 1. The resulting growth rate for an azimuthally propagating mode is shown in Fig. 3 as a function of normalized azimuthal wavenumber $k_y\lambda_D$.

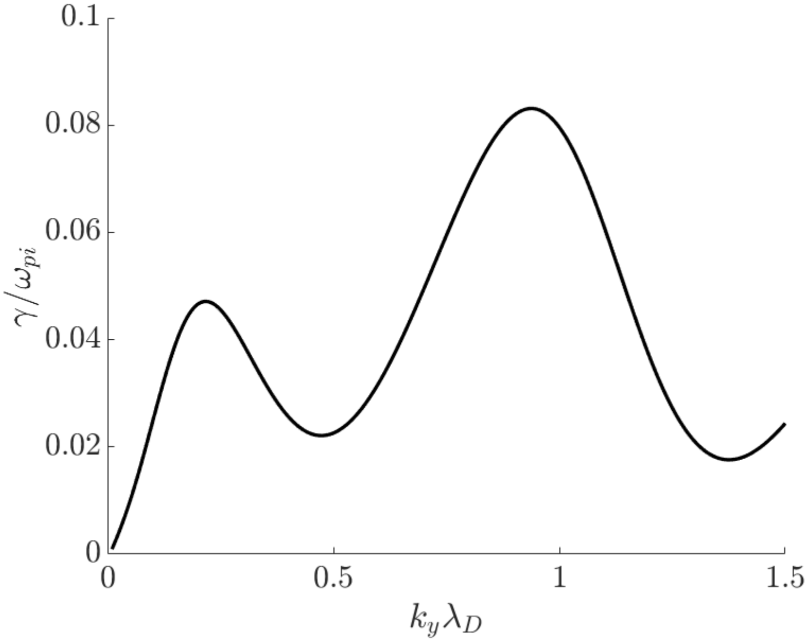

Figure 3. Growth rate of the ECDI and MTSI modes for $k_x\lambda_D = k_z\lambda_D = 0.0522$, where λ_D is based off of 25 eV electrons with density $5 \times 10^{16}\ m^{-3}$.

Because the domain length in each direction is 2 cm, this fixes the longest wavelength possible within the computational domain, hence limiting the maximum growth rate of the instability because the growth rate increases as the wavenumber perpendicular to the magnetic field decreases. For a purely azimuthally propagating mode in this 3D periodic box, the maximum growth rate for the MTSI mode should be $0.047\omega_{pi}$ at a wavenumber of $k_y\lambda_D = 0.22$. The maximum growth rate for the ECDI mode should be $0.083\omega_{pi}$ at a wavenumber of $k_y\lambda_D = 0.94$. Landau damping is expected to more strongly affect shorter wavelength modes,[18] so this ECDI mode should saturate rather quickly as the electrons and ions are heated by the plasma-wave interactions. It is important to emphasize that the analysis in Fig. 3 only applies for the linear growth stage of the instability, when the original plasma parameters are close to the ones given in Table 1. If an instability appears later into the simulation, the temperature of each species should be reevaluated at the current simulation time and used to inform the growth rate. The density of the plasma stays constant for this periodic case.

There are two main stages of instability development in this cross-field test case: a period of short-wavelength, azimuthal propagation during the first microsecond and a period of a long-wavelength, axial-azimuthal propagation following this. The two stages are illustrated by the ion density profiles in Fig. 4. The first stage of instability growth, illustrated in Fig. 5(a), is characterized by a purely azimuthally propagating mode with 18 wavelengths within the computational domain. This azimuthally propagating wave that the ions are experiencing is only present in the azimuthal component of the electric field, i.e., the $\mathbf{E} \times \mathbf{B}$ direction, as would be expected of ECDI. This mode corresponds to a normalized azimuthal wavenumber of $k_y\lambda_D = 0.94$. This provides excellent agreement with the ECDI peak shown in Fig. 3. The growth rate of the mode can also be calculated using Fig. 5. The slope of $\int \phi^2 dV$ as a function of time on a logarithmic scale provides an estimate for the computational growth rate. An estimate for the slope of

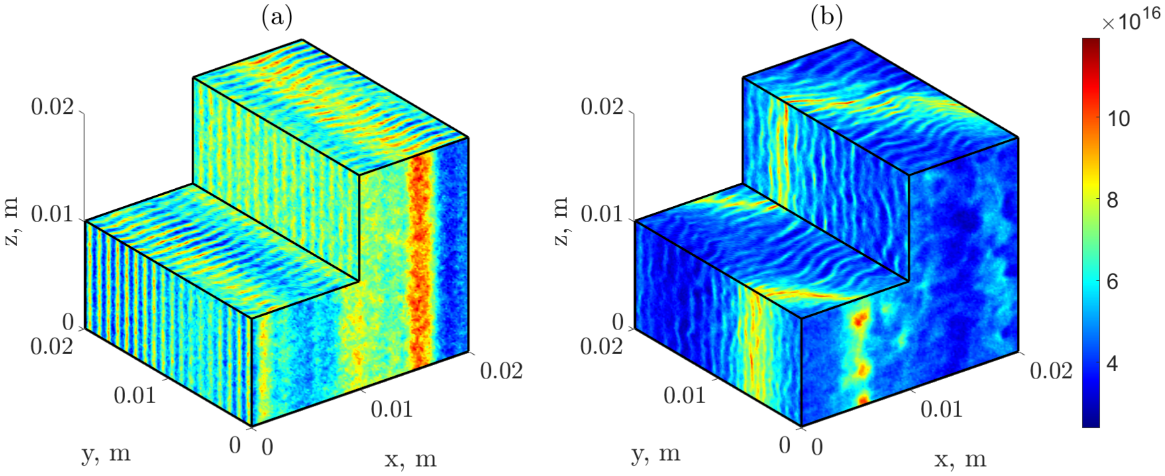

Figure 4. (a) Ion density at 0.28 μs, (b) Ion density at 1.6 μs.

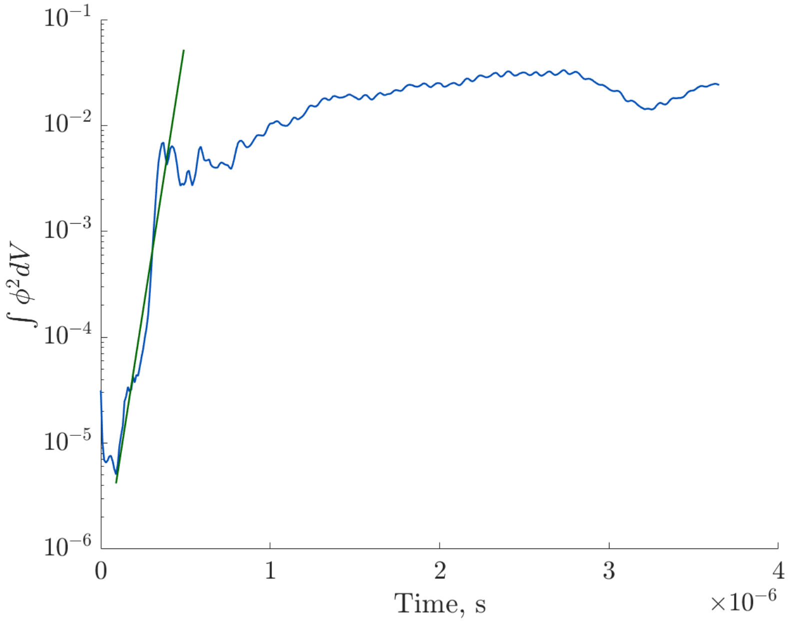

Figure 5. The blue line represents volume integrated ϕ^2 as a function of time. The green line represents the exponential fit for $\gamma = 0.08\omega_{pi}$.

$\int \phi^2 dV$ is given in Fig. 5, where it is demonstrated that a fit of $\gamma = 0.08\omega_{pi}$ provides good agreement for the early stages of the linear growth regime. Comparing this to the linear instability theory for the ECDI mode in Fig. 3, in which the analytical value of the growth rate is predicted to be $0.083\omega_{pi}$, this provides excellent evidence that this purely azimuthal mode is indeed ECDI.

Toward the end of the linear growth stage in Fig. 5, there is a short period of accelerated growth rate. This feature has been seen in other work, such as Chan, Hara, and Boyd.[19] This regime can be characterized by the spectrum filling in at non-harmonic wavenumbers as the instability saturates. This nonlinear phenomena causes super-linear growth before the instability saturates, so it cannot be predicted with linear perturbation theory alone.

The second phase of the instability in this test case begins with the emergence of a long-wavelength mode propagating at a 45° angle in the x-y plane. Because it is at an angle within the domain, the k_x and k_y values are the minimum allowable for the domain, i.e., $2\pi/L$ such that $k_x = k_y = 314$ rad/m. As a result, the total wavenumber is the slightly larger value of $k = \sqrt{2}k_x = 444$ rad/m. Here, the actual value of the wavenumber is used because at the time that this longer wavelength mode dominates the electrostatic energy within the system, the temperature is no longer 25 eV for electrons and 0.25 eV for ions. Instead, the electron temperature is closer to 100 eV within the wavefront, and the ion temperature is about 10 eV in the same location. As a result, the instability characteristic looks quite different from the condition shown in Fig. 3.

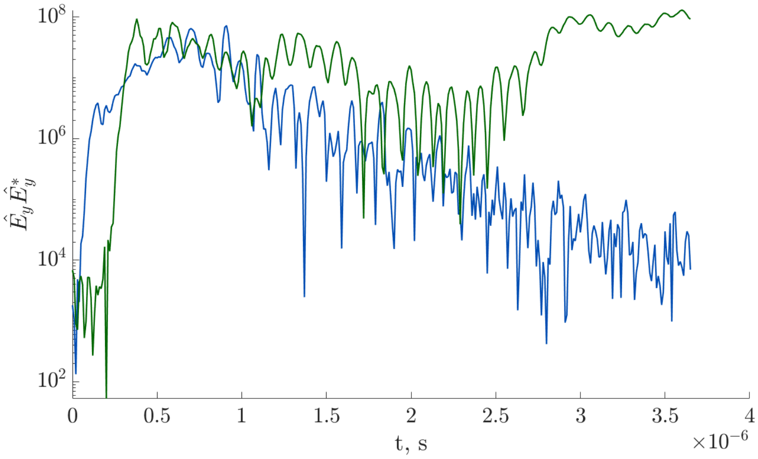

Figure 6. The energy spectrum of the electric field in the y-direction, calculated by the Fourier coefficients. The blue line is the ECDI mode, the green line is the long-wavelength mode.

This long-wavelength mode becomes dominant during the nonlinear saturation phase of the simulation, so linear theory is not valid to predict the growth rate and wavelength of the resulting modes, as the amplitude of the potential oscillations created by the electrostatic wave has already become large enough to allow particles to become trapped. This trapping facilitates the exchange of energy from the waves back into the particles' kinetic energy, stopping instability growth. Naively, the MTSI mode is expected to grow at a rate that is 40% slower than the ECDI mode, but this is not what is seen when analyzing the Fourier coefficients of the electric field in the y-direction, depicted in Fig. 6. At 1.6 μs, like in Fig. 4(b), the amplitude of the ECDI mode is still roughly 40% of the amplitude of the long-wavelength mode. However, at later simulation times, the ECDI mode experiences strong Landau damping as the ions and electrons heat up. After about 2.5 μs, amplitude of the ECDI mode is sufficiently damped compared to the long-wavelength mode. As the ECDI damps, energy is transferred back to the particles, which is then transferred by wave-particle interactions to the long-wavelength mode such that the electrostatic energy remains roughly constant for later times. This is most evident beyond 2.5 μs in Fig. 6.

The growth of the long-wavelength mode begins around 0.25 μs with the same growth rate as the ECDI mode earlier in the simulation. Once the linear ECDI growth saturates, the linear growth of the long-wavelength growth begins, indicating that these modes are exchanging energy with one another via the particles. It is not immediately clear that this long-wavelength mode is MTSI, because the linear theory for MTSI, presented in Eq. (2), is not valid during its growth stage. Further analysis needs to be undertaken to study the coupling between ECDI and MTSI in this context, or whether this wave corresponds to MTSI at all. From Fig. 4, it is clear that there is no z-component of the oscillation, yet a nonzero wavenumber component along the magnetic field is fundamental to the MTSI mode. Furthermore, more analysis needs to be conducted to determine how this mode acquires a nonzero component along the electric field. It is interesting to node that while the ECDI mode only has oscillations in E_y, the long-wavelength mode has equal amplitude oscillations in both E_x and E_y. If the bulk velocity of electrons has attained a significant value along the electric field, across magnetic field lines, by the influence of the ECDI mode, i.e., anomalous electric transport, this would Doppler shift the long-wavelength mode such that the direction of propagation is in the x-y plane rather than purely in the $-y$ direction. However, more data analysis is required to determine the explanation of this phenomenon.

V. Conclusion

In this study, a 3D PIC code was developed and verified using the two-stream instability test case for fixed ions. A 3D, periodic box with perpendicular, applied electric and magnetic fields was used as a platform to study the development of instabilities in partially magnetized, cross-field plasma discharges like Hall effect thrusters. Based on the initial plasma parameters, the short-wavelength mode that immediately develops is consistent with ECDI with respect to its wavelength and its growth rate. However, once this mode saturates, a longer wavelength mode takes over, whose characteristics do not perfectly match the characteristics of MTSI predicted by linear perturbation theory. However, this is to be expected for a wave being initiated in the nonlinear saturation regime of another instability. Evidence was shown through Fourier analysis that this long-wavelength mode is exchanging energy with this ECDI mode, coupling them together, fundamentally changing its behavior. More analysis is required to study the reason why the long-wavelength mode behaves as it does, but the quantitative agreement of the mode propagating in the $\mathbf{E} \times \mathbf{B}$ direction with the linear perturbation theory for ECDI provides an excellent first step to better understanding the nature of kinetic instabilities in Hall effect thrusters.

VI. Acknowledgements

This work was supported by a NASA Space Technology Graduate Research Opportunity, under Grant No. 80NSSC21K1273, and NASA through the Joint Advanced Propulsion Institute, a NASA Space Technology Research Institute under Grant No. 80NSSC21K1118. Finally, we would like to acknowledge Stanford University's HPCs for computational resources.

References

[1] I. D. Kaganovich, A. Smolyakov, Y. Raitses, E. Ahedo, I. G. Mikellides, B. Jorns, F. Taccogna, R. Gueroult, S. Tsikata, A. Bourdon, J.-P. Boeuf, M. Keidar, A. T. Powis, M. Merino, M. Cappelli, K. Hara, J. A. Carlsson, N. J. Fisch, P. Chabert, I. Schweigert, T. Lafleur, K. Matyash, A. V. Khrabrov, R. W. Boswell, and A. Fruchtman, "Physics of E×B discharges relevant to plasma propulsion and similar technologies," *Physics of Plasmas*, vol. 27, p. 120601, 12 2020.

[2] J. C. Adam, A. Héron, and G. Laval, "Study of stationary plasma thrusters using two-dimensional fully kinetic simulations," *Physics of Plasmas*, vol. 11, no. 1, pp. 295–305, 2004.

[3] A. Héron and J. C. Adam, "Anomalous conductivity in Hall thrusters: Effects of the non-linear coupling of the electron-cyclotron drift instability with secondary electron emission of the walls," *Physics of Plasmas*, vol. 20, p. 082313, 08 2013.

[4] S. Tsikata, J. Cavalier, A. Héron, C. Honoré, N. Lemoine, D. Grésillon, and D. Coulette, "An axially propagating two-stream instability in the hall thruster plasma," *Physics of Plasmas*, vol. 21, no. 7, p. 072116, 2014.

[5] T. Lafleur, S. D. Baalrud, and P. Chabert, "Theory for the anomalous electron transport in hall effect thrusters. ii. kinetic model," *Physics of Plasmas*, vol. 23, no. 5, p. 053503, 2016.

[6] S. Tsikata, N. Lemoine, V. Pisarev, and D. M. Grésillon, "Dispersion relations of electron density fluctuations in a hall thruster plasma, observed by collective light scattering," *Physics of Plasmas*, vol. 16, no. 3, p. 033506, 2009.

[7] D. W. Forslund, R. L. Morse, and C. W. Nielson, "Electron cyclotron drift instability," *Phys. Rev. Lett.*, vol. 25, pp. 1266–1270, Nov 1970.

[8] D. W. Forslund, R. L. Morse, and C. W. Nielson, "Nonlinear electron-cyclotron drift instability and turbulence," *Phys. Rev. Lett.*, vol. 27, pp. 1424–1428, Nov 1971.

[9] J. B. McBride, E. Ott, J. P. Boris, and J. H. Orens, "Theory and simulation of turbulent heating by the modified two-stream instability," *The Physics of Fluids*, vol. 15, no. 12, pp. 2367–2383, 1972.

[10] C. Lashmore-Davies and T. Martin, "Electrostatic instabilities driven by an electric current perpendicular to a magnetic field," *Nuclear Fusion*, vol. 13, pp. 193–203, mar 1973.

[11] W. Villafana, F. Petronio, A. C. Denig, M. J. Jimenez, D. Eremin, L. Garrigues, F. Taccogna, A. Alvarez-Laguna, J. P. Boeuf, A. Bourdon, P. Chabert, T. Charoy, B. Cuenot, K. Hara, F. Pechereau, A. Smolyakov, D. Sydorenko, A. Tavant, and O. Vermorel, "2d radial-azimuthal particle-in-cell benchmark for e×b discharges," *Plasma Sources Science and Technology*, vol. 30, p. 075002, jul 2021.

[12] T. Charoy, J. P. Boeuf, A. Bourdon, J. A. Carlsson, P. Chabert, B. Cuenot, D. Eremin, L. Garrigues, K. Hara, I. D. Kaganovich, A. T. Powis, A. Smolyakov, D. Sydorenko, A. Tavant, O. Vermorel, and W. Villafana, "2d axial-azimuthal particle-in-cell benchmark for low-temperature partially magnetized plasmas," *Plasma Sources Science and Technology*, vol. 28, p. 105010, oct 2019.

[13] J. Cavalier, N. Lemoine, G. Bonhomme, S. Tsikata, C. Honore, and D. Gresillon, "Hall thruster plasma fluctuations identified as the e×b electron drift instability: Modeling and fitting on experimental data," *Physics of Plasmas*, vol. 20, 08 2013.

[14] A. C. Denig and K. Hara, "Three-dimensional coupling of electron cyclotron drift instability and ion–ion two stream instability," *Physics of Plasmas*, vol. 30, p. 032108, 03 2023.

[15] F. Taccogna and P. Minelli, "Three-dimensional particle-in-cell model of Hall thruster: The discharge channel," *Physics of Plasmas*, vol. 25, p. 061208, 06 2018.

[16] W. Villafana, B. Cuenot, and O. Vermorel, “3D particle-in-cell study of the electron drift instability in a Hall Thruster using unstructured grids,” *Physics of Plasmas*, vol. 30, p. 033503, 03 2023.

[17] R. D. Falgout and U. M. Yang, “hypre: A library of high performance preconditioners,” in *Computational Science — ICCS 2002* (P. M. A. Sloot, A. G. Hoekstra, C. J. K. Tan, and J. J. Dongarra, eds.), (Berlin, Heidelberg), pp. 632–641, Springer Berlin Heidelberg, 2002.

[18] A. Ducrocq, J. C. Adam, A. Héron, and G. Laval, “High-frequency electron drift instability in the cross-field configuration of hall thrusters,” *Physics of Plasmas*, vol. 13, no. 10, p. 102111, 2006.

[19] W. H. R. Chan, K. Hara, and I. D. Boyd, “Effects of multi-dimensionality and energy exchange on electrostatic current-driven plasma instabilities and turbulence,” *Journal of Plasma Physics*, vol. 90, no. 2, p. 905900206, 2024.